High resolution (NA = 0.8) in lensless in-line holographic microscopy with glass sample carriers

Mario Kanka,* Rainer Riesenberg, Paul Petruck, and Christian Graulig

Institute of Photonic Technology, Albert-Einstein-Str. 9, 07747 Jena, Germany

**Corresponding author: mario.kanka@ipht-jena.de*

Received May 27, 2011; revised July 15, 2011; accepted August 10, 2011;
posted August 17, 2011 (Doc. ID 148331); published September 14, 2011

For lensless digital in-line holographic microscopy a new state-of-the-art spatial resolution corresponding to an NA of 0.8 is shown based on the tile superposition propagation. The result is proved using a common glass sample carrier with a refraction index of 1.52. Single-shot high-resolution imaging is possible by suppression of coherent reflections in an optimized arrangement using partially coherent laser light illumination.

OCIS codes: 090.1000, 090.1995, 180.0180.

In-line holographic imaging, invented by D. Gabor, can be implemented with a very simple experimental setup [1]. In lensless digital in-line holographic microscopy (DIHM) only the following components are needed: a coherent light source, a pinhole, a digital image sensor, and a computer [2,3]. Pinholes with diameters in the range of the wavelength generate a spherical wavefront, which is needed to overcome a resolution limitation caused by the pixel pitch of the image sensor [4–6]. This spherical wavefront is partially scattered by a sample to be imaged. The resulting hologram is digitally recorded by the image sensor and an image of the sample is reconstructed numerically on a computer.

Today DIHM is well established for lensless imaging of microscopic samples [4–10]. Because a complex wave field scattered by a sample is reconstructed, one 2D hologram contains the optical information about the sample in a 3D volume. For practical applications the reconstruction of the wave field must be efficient and fast. The widely used Fresnel transform is only applicable under paraxial conditions, i.e., for low NAs. Thus, the spatial resolution in the reconstructed microscopic images is restricted, too. Reconstruction techniques based on coordinate transforms to spherical surfaces are more suitable for DIHM [11,12] and enable lensless microscopic imaging with an NA of about 0.5 [4]. To improve the NA, different strategies generating synthetic apertures (SA) were published in recent years. In lensless DIHM with SA, an image resolution according to an NA of 0.7 was achieved [9]. But its application is restricted to stationary or slowly moving samples due to the need for multiple exposures. A single exposure SA by coherence- [13], polarization- [14], or color-multiplexing [15] increases the complexity of the setup, where further optical elements become necessary.

In this Letter, we will show that an optical resolution according to an NA of 0.8 can be reached with simple lensless DIHM setups as described above. The reconstruction technique needed is based on the tile superposition propagation implementing the first Rayleigh–Sommerfeld integral for free space propagation of light between parallel planes [5]. The numerical complexity equals that of a fast Fourier transform of the hologram and is independent of the object image resolution [6]. Today commercial digital image sensor chips generally have edge lengths of 4…24 mm. Thus, to achieve larger NAs with values of about 0.8 would lead to accordingly short detection distances of only a few millimeters (refraction index $n = 1$). At the same time, usual pixel pitches of 1.7…14 μm exceed half of the wavelength of visible light. A high-resolution lensless DIHM with commercial image sensor chips leads to very compact setups with pinhole to sensor distances of only a few millimeters. According to the sampling theorem of Nyquist–Shannon, very short distances of only a few hundred micrometers between pinhole and sample become necessary to detect holograms without aliasing. To realize such short distances, the sample carrier (a glass slide) is introduced between the pinhole and image sensor in such a way that the sample is facing the pinhole, shown in Fig. 1. This approach also reduces coherent reflections and glass aberrations as described in the following.

The diffraction pattern of a monochromatically illuminated pinhole is described by the Airy function. Pinholes with diameters less than 1.22λ diffract incoming light of wavelength λ into spherical wavefronts. A thin glass slide serves as the sample carrier. At the surface of the sample carrier the light will be partially reflected back to the (high reflective) pinhole chip, which in turn reflects this light almost completely back to the sample carrier, where it is partially reflected back again. As a result, light

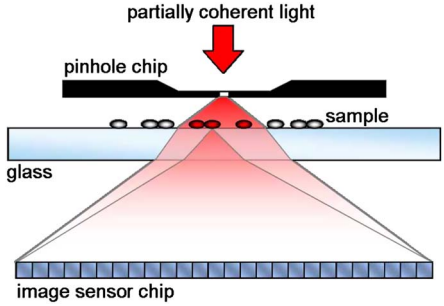

Fig. 1. (Color online) Lensless digital in-line holographic microscopy.

coming directly from the pinhole will be superposed by the reflected light, which then appears to come from several virtual pinholes. If all these wavefronts are coherent, the hologram will be considerably disturbed by additional concentric ring patterns, as shown in Fig. 2(a). To avoid this, the length of temporal coherence l_{coh} should be limited so that the hologram wave and the multiply reflected light are practically incoherent. On the other hand, the coherence length must exceed the path difference between the light coming directly from the pinhole and the light scattered by the object. For high NA holograms the optical path difference can approach values as large as the distance z_{obj} from pinhole to sample. The temporal coherence length l_{coh} must exceed such maximum path differences. From both conditions follows

$$z_{\mathrm{obj}} \le l_{\mathrm{coh}} < 2z_{\mathrm{glass}}, \tag{1}$$

where z_{glass} is the distance between the surfaces of the pinhole chip and the sample carrier. As long as the thickness h of the sample carrier exceeds $z_{\mathrm{obj}}/2$, the sample must be facing the pinhole to fulfill in Eq. (1), as shown in Fig. 2(b). Internal reflections between the two sample carrier surfaces as well as reflections between the sample carrier and the image sensor are too weak compared to the hologram wave and hence do not need to be considered. If the sample is facing the image sensor, as shown in Fig. 2(a), the sample carrier influences only the pinhole wave, but not the diffraction pattern of the sample. The pinhole wave serves as the reference in the hologram reconstruction process and hence must be known. Thus, the refraction index as well as the thickness of the sample carrier must be considered, too. In the approach proposed here, where the sample faces the pinhole [Fig. 2(b)], the sample carrier influences the complete hologram wave. However, a thin sample carrier (compared to the distance between the pinhole and the image sensor) causes only a negligible distortion of the hologram.

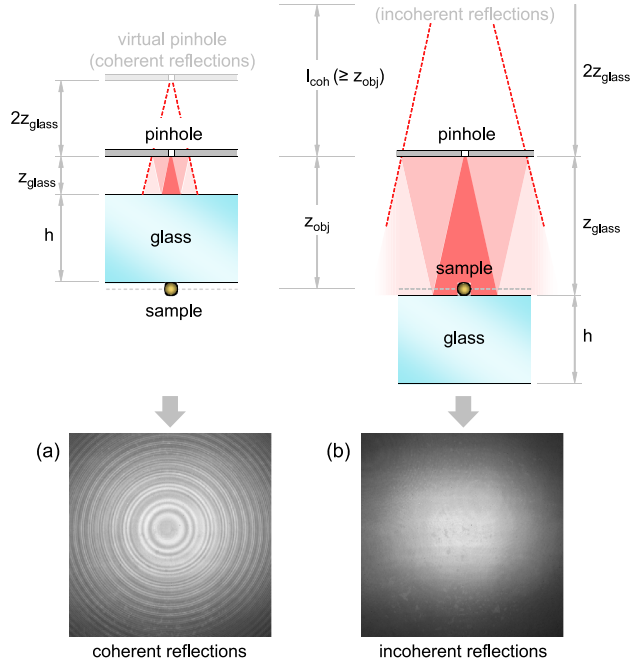

Fig. 2. (Color online) Multiple reflections between pinhole chip and sample carrier (glass) using light sources with limited temporal coherence. (a) If the pinhole to sample carrier distance is too little, these reflections cause disturbing additional concentric ring systems in the measured hologram (below). (b) By turning the sample carrier upside down, the distance is increased and the reflections become practically incoherent. The measured hologram (below) is free from disturbing interferences.

In the experimental setup, a fiber-coupled diode laser of wavelength $\lambda = 661\,\mathrm{nm}$ (TOPTICA iPulse) in continuous wave mode with an output power of 10 mW is used as the light source. The diode current is internally modulated by a sinusoidal frequency of 130 MHz within an amplitude range of 80%. Therefore, every longitudinal mode starts oscillating under nearly equal conditions within the amplification range of the laser medium and cavity. Consequently, the emitted light is composed of several wavelengths and yields an effective bandwidth of the almost Lorentz-shaped spectrum of about 1.2 nm. Thus, the length of temporal coherence is reduced to 166 μm at an interference contrast of 50%. We use a pinhole of a diameter of about 650 nm drilled into a thin membrane by means of e-beam lithography. The metalized surface of this membrane is highly reflective. A monochrome image sensor chip (complementary metal oxide semiconductor, Cypress Semiconductor Corporation, IBIS-A-6600) with a pixel pitch of 3.5 μm is used to record holograms with 2048×2048 pixels. The protection glass of this sensor was removed to avoid additional reflections and aberrations. The sensor's package dimensions limit the minimum distance between the sample carrier and sensor area to 1.5 mm. The sample carrier is a thin cover glass commonly used in optical microscopy.

A suspension of 816 nm ($\pm$20 nm) poly methyl methacrylate (PMMA) beads was dropped on the sample carrier. While the droplet was drying up, the beads formed hexagonally aligned 2D clusters [Fig. 3(a)]. The tile superposition propagation reconstructs four megapixel holograms in approximately 4 s [5]. The influence of the glass sample carrier with a thickness of 170 μm and a refraction index of 1.52 was corrected numerically by an additional propagation of the rescaled object image. Figure 3(d) shows reconstructed bead clusters. The distance from the pinhole to the image sensor was determined to be 2045 μm. The distance between the pinhole and the sample was 131 μm. In theory, to resolve a grating period of $\delta = 816\,\mathrm{nm}$, an NA of 0.81 is needed, where $\mathrm{NA} = \lambda/\delta$ (Abbe) and $\lambda = 661\,\mathrm{nm}$. To verify the realized NA, the reconstructed image was numerically filtered according to different NA values. The images for NA = 0.9 and NA = 0.85 are identical, but contrast is lost for NA = 0.8. So an NA of at least 0.8 was realized [see Fig. 3(f)]. Figures 3(g) and 3(h) (pinhole to sample distance 219 μm) show a biological sample with similar image quality.

As explained above, the thin sample carrier causes only a neglectable distortion of the hologram, which was, however, corrected. Alternatively to this correction, a slight change in the pinhole to sensor distance to 2000 μm is necessary to reconstruct an image of comparable

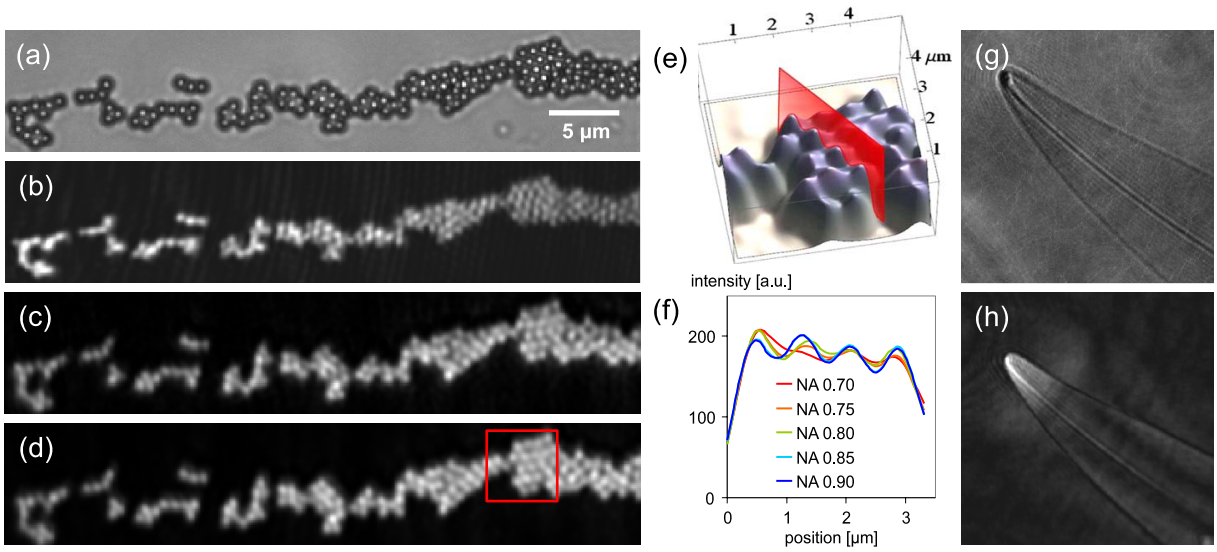

Fig. 3. (Color online) (a) 816 nm PMMA beads (±20 nm) imaged by an optical microscope (NA 0.75, $\lambda = 470$ nm). (b) Reconstructed DIHM image of the same scene using a highly coherent laser and (c) a partially coherent laser. (d) The same DIHM image after an additional numerical correction of the glass sample carrier. (e) 3D view of the red framed image section in (d). (f) Sectional view for different NAs, as indicated in (e). (g) Pleurosigma angulatum imaged by an optical microscope (NA 0.75, $\lambda = 661$ nm) and (h) the DIHM image with similar quality.

quality [Fig. 3(c)]. Most of the beads are resolved in both images, but to resolve all these hexagonally aligned beads with a distance of 816 nm to each other, an NA of 0.94 is needed and could be achieved by shortening the distance between the pinhole and the image sensor, which unfortunately was not possible with the present setup.

In lensless in-line holographic microscopy with high image resolution, very compact setups with pinhole to sensor distances of only a few millimeters are used. According to this, very short pinhole to sample distances of only a few hundred micrometers become necessary. In the present setup a partially coherent light source is used and the glass sample carrier is introduced between pinhole and image sensor in such a way that the sample is facing the pinhole. This approach enables arbitrarily short pinhole to sample distances and reduces coherent reflections and glass aberrations at the same time. The tile superposition propagation reconstructs images of several megapixels in only a few seconds using common desktop computers. 816 nm PMMA beads were resolved using an illumination wavelength of $\lambda = 661$ nm. The spatial resolution in lensless in-line holographic microscopy is extended according to NAs of 0.8.

We thank H. J. Kreuzer for his support and critical reading of the manuscript.

References

1. D. Gabor, Nature **161**, 777 (1948).
2. J. W. Goodman and R. W. Lawrence, Appl. Phys. Lett. **11**, 77 (1967).
3. H.-W. Fink, H. Schmid, H. J. Kreuzer, and A. Wierzbicki, Phys. Rev. Lett. **67**, 1543 (1991).
4. J. Garcia-Sucerquia, W. Xu, S. K. Jericho, P. Klages, M. H. Jericho, and H. J. Kreuzer, Appl. Opt. **45**, 836 (2006).
5. M. Kanka, R. Riesenberg, and H. J. Kreuzer, Opt. Lett. **34**, 1162 (2009).
6. M. Kanka, A. Wuttig, C. Graulig, and R. Riesenberg, Opt. Lett. **35**, 217 (2010).
7. D. Tseng, O. Mudanyali, C. Oztoprak, S. O. Isikman, I. Sencan, O. Yaglidere, and A. Ozcan, Lab Chip **10**, 1787 (2010).
8. T. Meinecke, N. Sabitov, and S. Sinzinger, Appl. Opt. **49**, 2446 (2010).
9. V. Micó and Z. Zalevsky, J. Biomed. Opt. **15**, 046027 (2010).
10. M. Paturzo and P. Ferraro, Opt. Express **17**, 20546 (2009).
11. H. J. Kreuzer, K. Nakamura, A. Wierzbicki, H.-W. Fink, and H. Schmid, Ultramicroscopy **45**, 381 (1992).
12. Y. Takaki and H. Ohzu, Appl. Opt. **38**, 2204 (1999).
13. V. Micó, Z. Zalevsky, P. Garcia-Martinez, and J. Garcia, Opt. Express **12**, 2589 (2004).
14. J. Zhao, X. Yan, W. Sun, and J. Di, Opt. Lett. **35**, 3519 (2010).
15. A. Calabuig, V. Micó, J. Garcia, Z. Zalevsky, and C. Ferreira, Opt. Lett. **36**, 885 (2011).